

# Fluid-body interaction on a Cartesian grid: dedicated studies for a CFD validation

G. Colicchio\*      M. Greco\*      O. M. Faltinsen\*\*  
g.colicchio@insean.it    m.greco@insean.it    oddfal@marin.ntnu.no

\* INSEAN, Italian Ship Model Basin, Roma – Italy.

\*\* Centre for Ships and Ocean Structures, NTNU, Trondheim – Norway.

CFD methods are getting more and more popular to investigate applications in Fluid Dynamics. This is because of their versatility and robustness. An important issue for them is to assess the results sensitivity to the involved parameters, their physical correctness and accuracy. Especially if a Cartesian grid is adopted, the fluid interaction with generally shaped bodies is a challenging problem. In this framework the presence of a fluid interface complicates the numerical difficulties. Generally speaking, errors in the enforcement of the body-boundary conditions will affect both the kinematics and dynamics. The sensitivity of the numerical solution to such errors depends on the examined problem. Figure 1 shows two practical examples: (i) the flooding phenomenon across a road and (ii) a freely floating ship in waves. In case (i), the water interaction with the terrain affects ve-

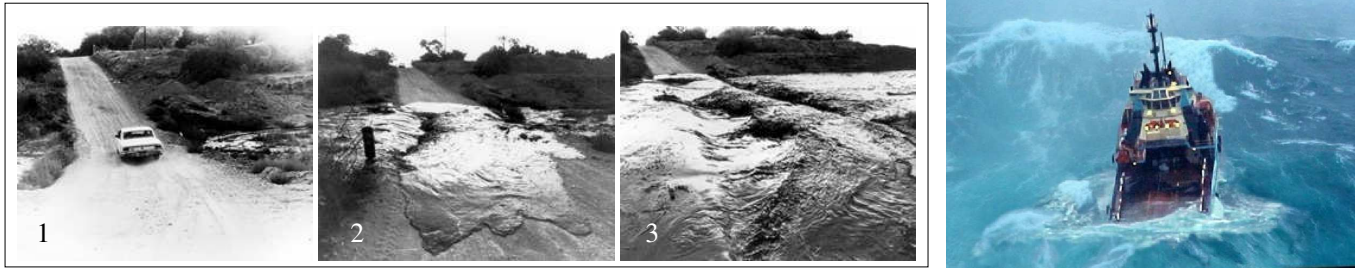


Figure 1: Left: flooding phenomenon. 1: dry road. 2: water reaches the road from the left. 3: the road is interrupted by the flooding. Right: large wave-ship interaction.

locity and direction of the liquid propagation. In this case the boundaries are fixed and the description of the kinematics is of main concern. Differently, in case (ii) the numerical capability to handle the pressure field plays a crucial role because the body motions are coupled with the fluid dynamic problem.

Here the Navier-Stokes solver by Colicchio (2004) has been taken as CFD method to assess the prediction of kinematic and dynamic variables. The solver is combined with a Level-Set technique to handle the interface evolution, when present, and simulates both liquid and gaseous phases assuming them as incompressible fluids. A second-order finite-difference scheme on a Cartesian fixed staggered grid is employed. This is combined with a Projection method to solve the governing equations. Time integration is performed by a second order predictor-corrector algorithm. The presence of a solid boundary is handled by introducing a second Level-Set function  $\psi$  defined (on the grid points) as the distance with sign from the body surface.  $\psi$  is positive in the points outside the body and negative otherwise. Moreover, as the air-water interface is smoothed using the related Level-Set function  $\phi$ , also the body boundary is smoothed applying a smoothing with  $\psi$  between the fluid Navier-Stokes equations and the body equations of motion within a layer  $\pm\delta_B$  across the body. Consistently the velocity goes smoothly from the fluid to the body values, and *vice versa*. This means that a relaxed no-slip condition is enforced. To handle the contact point between the air-water interface and the body, locally near the solid boundary  $\phi$  is prolonged symmetrically. Such extension is fundamental to reconstruct correctly the interface near the structure and is a quite complex task for generally shaped fixed/moving bodies.

To focus on the influence of the numerical parameters and grid discretization, problems with increasing complexities have been analyzed. First, three simple cases of water-structure impacts with restrained body motions were assumed (see left sketches in figure 2): the impact of a jet against a flat-rigid wall (case A), against a concave-rigid wall (case B) and against a convex-rigid wall (case C). Right table of figure 2 defines the numerical simulations performed for the three problems. Case A was used to investigate the smoothing parameters, *i.e.* functional law, application strategy and thickness  $2\delta_B$ . Cases B and C were selected to examine the effect of the parameter  $dx/R$ ,  $dx=dy$  being the grid discretization and  $1/R$  the local curvature. In all cases the gravity, the surface tension effects and the viscosity are neglected, one assumes a water jet surrounded by air, and  $V = 1$  is used as initial velocity of the jet. For the concave and convex bodies, the radius  $R$  of the solid cavities were taken equal to  $16 dx_m$ , with  $dx_m$  the reference discretization. In all simulations  $dt$  has been chosen equal to  $0.2 dx/V$ , fulfilling the stability requirements (see Colicchio 2004).

Figure 3 analyzes case A. In particular, the left plot shows two numerical simulations of the flow evolution assuming  $s = 16 dx$  as initial thickness of the jet. When a classical sinusoidal function is used (see left part of the plot) a jet parallel to the wall develops after the initial impact of the water against the structure. Because the capillary effects are not modeled and the local resolution is not sufficient, only the numerical errors can cause the merging of the jet to the body. This is also suggested by the large values reached by the mass-conservation error and by its irregular evolution, as reported in the right plot (case A2). The numerical solution is improved by modifying the smoothing function across the body (see right part of the left plot and case A5 in the right plot), in particular the sine is substituted with its tangent at  $\psi = +0.3\delta_B$  from such value of  $\psi$  until  $\psi = -\delta_B$ . Both

	$\delta_B$	smoothing function	mirroring	$R/dx_m$	$s/dx_m$
A1	1.0	modified sine	$\phi$	//	16
A2	1.5	sine	$\delta\phi/\delta t$	//	16
A3	2.0	modified sine	$\delta\phi/\delta t$	//	16
A4	2.5	modified sine	$\delta\phi/\delta t$	//	16
A5	1.5	modified sine	$\delta\phi/\delta t$	//	16
A6	1.0	modified sine	$\delta\phi/\delta t$	//	16
B1	1.5	modified sine	$\delta\phi/\delta t$	16	10
B2	1.5	modified sine	$\delta\phi/\delta t$	36	20
C1	1.5	modified sine	$\delta\phi/\delta t$	16	10
C2	1.5	modified sine	$\delta\phi/\delta t$	16	20

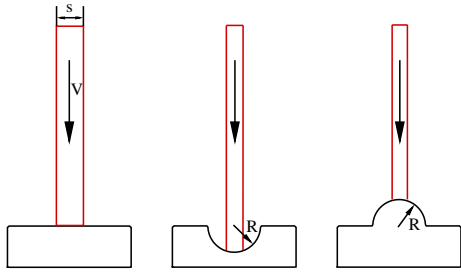


Figure 2: Left: problems used in the numerical analysis: impact of a jet with a flat-rigid wall (left), with a concave-rigid wall (center) and with a convex-rigid wall (right). Right: numerical tests for the three problems.

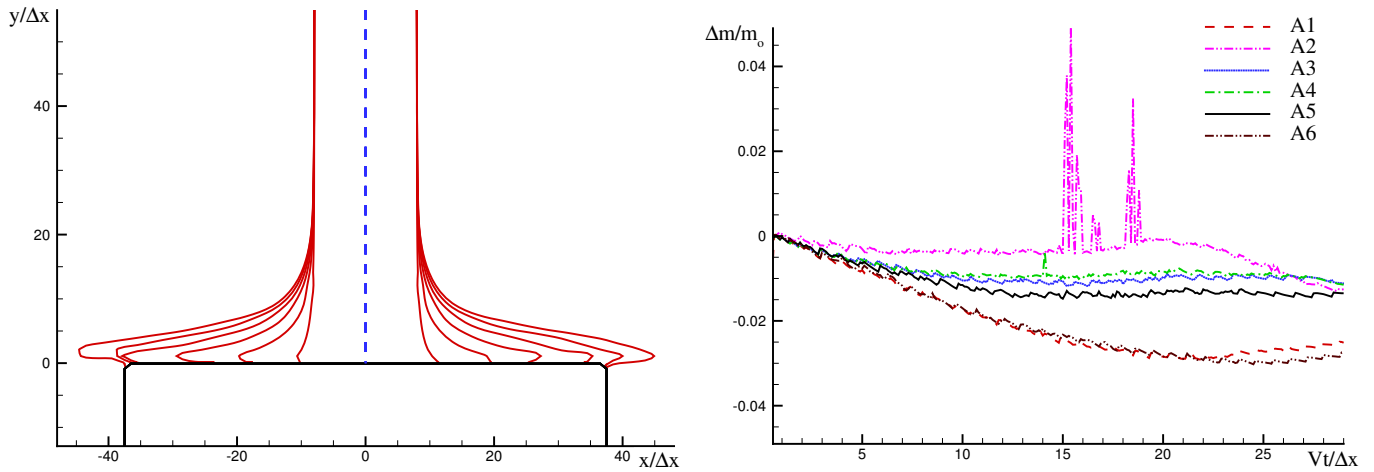


Figure 3: Results for case A. Left: jet evolution when a sine (left, case A2) and a modified-sine (right, A5) function are used for the smoothing. Right: mass time histories, where  $t$  is the time. The runs are defined in the right table of figure 2.

simulations have been performed with  $dx = dx_m$  and  $2\delta_B = 1.5 dx$ . Moreover, rather than  $\phi$ ,  $\partial\phi/\partial t$  is extended inside the body. The latter recipe improves the local accuracy of the solution (*i.e.* the description of the jet tip) and handles better the problem kinematics. Differently, its advantages are irrelevant in terms of mass conservation (compare cases A1 and A6 in the right plot). The mass-conservation error can be affected instead by  $\delta_B$  and, in particular, is smaller for thicker smoothing layers. From the results, for  $\delta_B \geq 1.5 dx$  the mass sensitivity to such parameter is limited and the related error is of the order of the numerical error made when evaluating the mass.  $\delta_B$  must be sufficiently large for a stable and accurate solution but sufficiently small to ensure a correct handling of the no-slip condition when the mesh is sufficiently fine to model the boundary layer. Therefore from the results  $2\delta_B = 1.5 dx$  can be taken as the best compromise.

The findings from case A have been used when studying the other problems. Case B is discussed in figure 4. The top-left plot gives the fluid evolution respectively for  $dx/R = dx_m/R = 1/16$  and  $dx/R = 1/32$ . Both discretizations describe correctly the kinematics of the problem. In particular they handle the upward jet leaving tangentially the wall after the impact and predict a jet toe that moves little and remains close to the edge of the cavity (see also top-center and top-right plots). However  $dx/R = 1/16$  is too large to handle the evolution of the jet apex. The latter should follow the tangent straight path from the edge of the cavity. The finer discretization can capture this behavior, consistently with the numerical description of the body geometry. As expected, when the discretization is halved (see bottom-left plot) the mass error reduces with a factor 2. However the slope of the corresponding curve is not particularly affected because for both simulations the committed error is of the order of the error due to the numerical prediction of the mass. The pressure evolution along the wall (see thick-solid lines in the bottom-right plot, case B1) is globally correct, with an initial rise at the inner region of the body and a later weak increase at the sides. The former is due to the initial impact of the jet and the latter is connected with the body concave shape that works against the flow caused along the structure by the impact. However the pressure curve is affected by numerical oscillations that are weakened by smaller  $dx/R$  (not given here) and are connected with the use of a grid independent from the body geometry. Moving toward the fluid the oscillations reduce and disappear, as it is shown by the pressure evolutions along lines distant half (thin-solid lines) and one

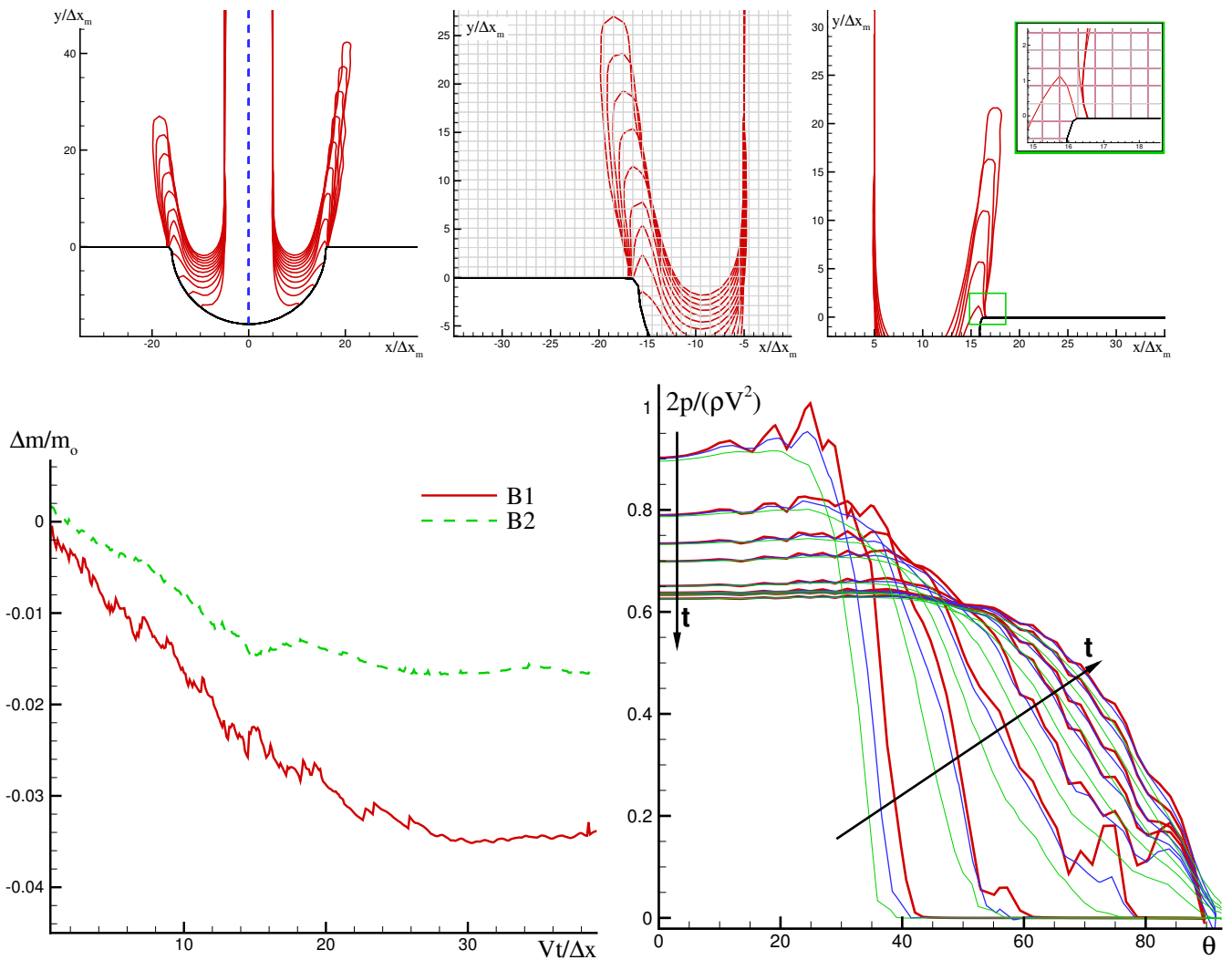


Figure 4: Results for case B. Top-left: jet evolutions for B1 (left) and B2 (right). Top-center: enlarged view of the later jet for B1, the used grid is also shown. Top-right: enlarged view of the later jet for B2 and detail showing the used grid and the position of the jet toe. Bottom-left: time history of the mass-conservation error.  $m_0$  is the initial mass. Bottom-right: pressure evolution along the body (thick-solid lines), at half cell (thin-solid lines) and at one cell (dashed lines) from the body for B1.  $\theta$  is the polar coordinate along the sloped portion of the body and  $t$  is the time. The runs are defined in the right table of figure 2.

(dashed lines) cell from the body. The results suggest that the unphysical oscillations are connected with the geometry of the grid and could be avoided by staggering the solution. This will be investigated at the workshop.

Case C is examined in figure 5. The left and center plots give, respectively, the fluid evolution and the pressure time history along the structure for  $dx/R = dx_m/R = 1/16$  and  $s = 20 dx$ , and for  $s = 10 dx$ . The used mesh describes correctly the kinematics

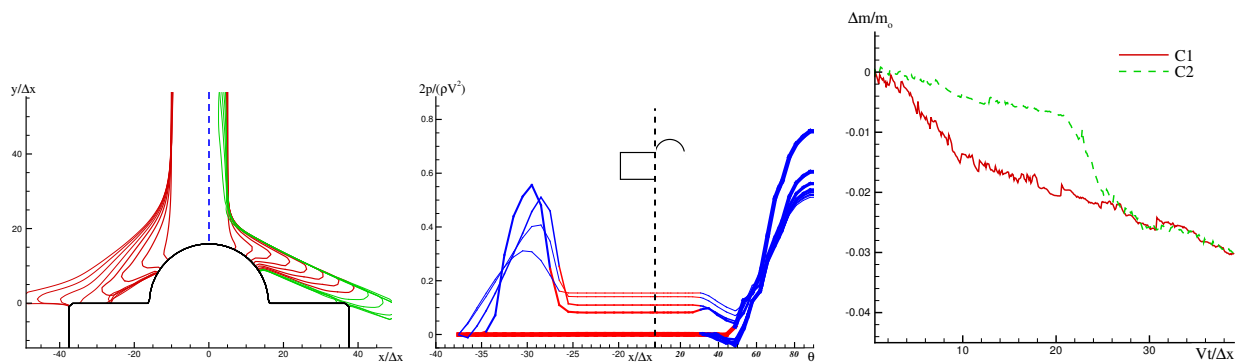


Figure 5: Results for case C. Left: jet evolutions for C1 (left) and for C2 (right). Center: evolution of the pressure along the body for C1.  $\theta$  is the polar coordinate along the sloped portion of the body and  $x$  the Cartesian coordinate along the flat portion. Right: time history of the mass-conservation error.  $m_0$  is the initial mass. The runs are defined in the right table of figure 2.

for both jet thicknesses. Generally, after the impact a jet flow develops along the structure and eventually detaches from it keeping the direction of the local tangent at the sloped wall. The thickest jet leaves the body at an angle slightly larger, hits the flat portion

of the wall and causes the formation of an air cavity. After this second impact another jet flow develops eventually detaching tangentially from the flat region. For this geometry very small oscillations are visible in the pressure curves. This is because the convex shape of the body supports the motion of the jet along the wall after the initial impact. Therefore in the sloped portion of the body only an initial central pressure rise occurs (see center plot). A later important pressure increase is documented in the flat portion of the wall once the jet has detached from it. Such rise is not observed for the thinnest jet while the other observations remain valid. In this case the jet detaches from the sloped wall with a direction sufficient to avoid the impact with the flat region (see right part of the left plot). The latter is just touched by the jet that maintains its direction. Also in this case a cavity is entrapped. During the initial stages of the evolution the thinnest jet is associated with a smaller mass loss but later on the errors committed in the two examples of case C become comparable (see right plot). The influence of the numerical parameters on the air cavity evolution will be analyzed at the workshop.

The effect of using a Cartesian fixed grid for a moving body is investigated in figure 6. A circular cylinder in an infinite

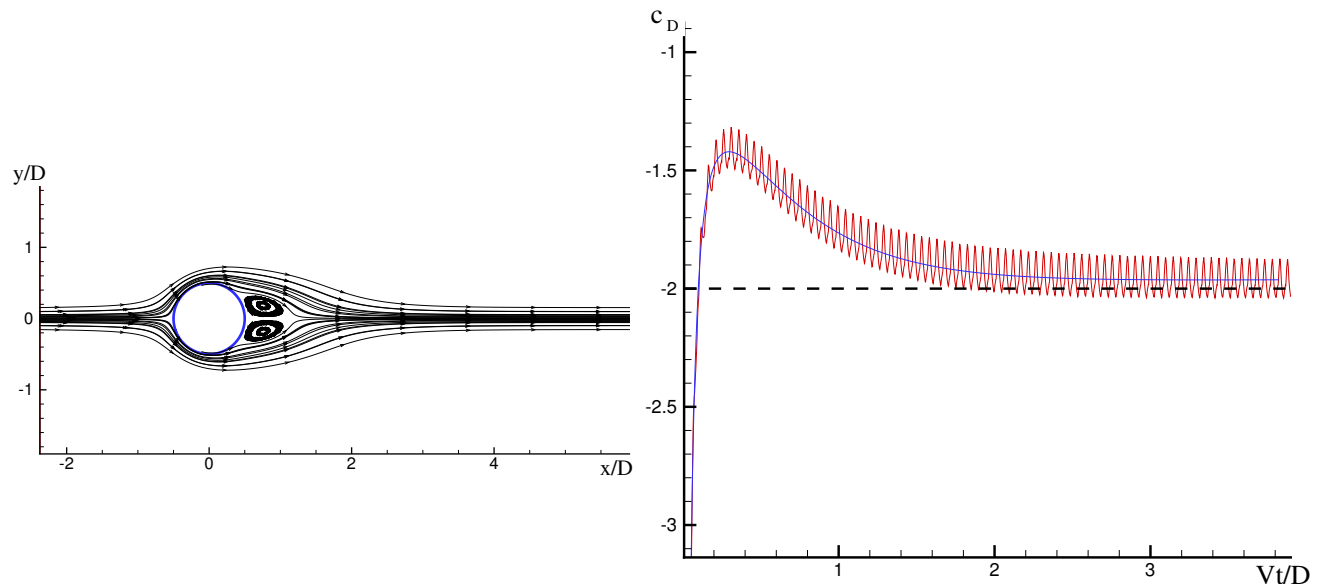


Figure 6: Circular cylinder with  $Re = 20$ . Left: definition of the problem and streamlines.  $D$  is the cylinder diameter. Right: evolution of the resistance coefficient on the cylinder. Solid line: numerical solution for the fixed cylinder. Dotted line: numerical solution for the moving cylinder. Dashed horizontal line: experiments by Tritton (1959).

fluid (see left sketch) and with a Reynolds number  $Re = 20$  is studied numerically in two alternative ways, by considering: (i) a current past a fixed cylinder and (ii) a cylinder moving in a fluid initially at rest. In both simulations  $dx/D = 1/22$  has been used, with  $D$  the cylinder diameter. For the considered Reynolds number, the body wake develops symmetrically and reaches a steady condition. Therefore the cylinder is subjected only to a resistance which is globally captured by both simulations. This is confirmed by the right plot of the figure showing the numerical evolutions of the load and the steady experimental value by Tritton (1959). However case (i) shows clear oscillations. The latter are connected with the passage of cells, due to the body motion, from inside to outside the solid or *vice versa*. More comparisons between the two systems of reference will be shown at the workshop in terms of the stagnation pressure, contributions from shear forces and pressure forces, separation point and length of the recirculating zone (see Zdravkovich 1997).

The challenges and numerical recipes discussed here are valid for the solver examined, but the base difficulties are common to CFD methods using Cartesian fixed grids. In particular, those connected with the occurrence of numerical load oscillations. If the body motions are coupled with the fluid dynamic problem such oscillations could worsen or even destroy the description of the water-structure interaction. Alternative numerical techniques aiming to avoid these oscillations, for example solving the system on two staggered grids, will be discussed at the workshop.

The present research activity is partially supported by the Centre for Ships and Ocean Structures, NTNU, Trondheim, within the "Green Water Events and Related Structural Loads" project, and partially done within the framework of the "Programma di Ricerca di Idrodinamica Navale 2005-2007" funded by *Ministero Infrastrutture e Trasporti*.

## References

- COLICCHIO, G. (2004). *Violent disturbance and fragmentation of free surfaces*. Ph. D. thesis, School of Civil Engineering and the Environment, University of Southampton, Southampton.
- TRITTON, D. J. (1959). Experiments on the flow past a circular cylinder at low Reynolds numbers. *J. Fluid Mech.* 16, 547–567.
- ZDRAVKOWICH, M. M. (1997). *Flow around Circular Cylinders, Vol.1: Fundamentals*. Oxford Science publications.